SPE 93951-PP

Modeling Long-Term CO_2 Storage in Aquifer with a Black-Oil Reservoir Simulator

Sjur Mo SPE and Idar Akervoll SPE, SINTEF Petroleum Research

This paper was prepared for presentation at the 2005 SPE/EPA/DOE Exploration and Production Environmental Conference held in Galveston, Texas, U.S.A., 7 – 9 March 2005.

Abstract

This paper presents results of modeling long-term CO_2 storage in a shallow saline aquifer with a commercial black-oil reservoir simulator. Realistic CO_2/water phase behavior (pVT properties) covering all pressure, temperature and compositional conditions accounted for during the simulations have been used. The pressure and temperature in the aquifer is above the CO_2 supercritical conditions giving rise to the existence of a two-phase fluid system of CO_2 as a supercritical fluid ("gas") and CO_2 dissolved in the aqueous phase. The objective was to model scenarios of CO_2 storage in aquifer with emphasis on the sensitivity of CO_2 distribution in the deposit with respect to critical CO_2 saturations during the injection period and to residual CO_2 saturation for water reentering CO_2 filled volumes (hysteresis in fluid saturations). The re-distribution of water occurs after stop of CO_2 injection due to gravity segregation of dense CO_2 saturated water and CO_2-free water. The impact of various reservoir parameters has been studied, including average permeability, vertical to horizontal permeability ratio (k_v/k_h), relative permeability, and capillary pressure. For the saturation functions the main focus has been on end points and hysteresis effects. It is observed that storage of CO_2 as residual gas is most important for low k_v/k_h ratios.

Introduction

The concentration of carbon dioxide (CO_2) continues to increase in the atmosphere as a result of CO_2 release from anthropogenic sources including burning of fossil fuels. The atmospheric concentration of CO_2 has increased from the pre-industrial age level of about 280 ppm to 370 ppm today[1]. This value is higher than the concentrations observed over the last 400 000 years.

The current emissions of CO_2 into the atmosphere exceed the capacity of the natural CO_2 cycling system to absorb the emissions. Accumulation of CO_2 and other greenhouse gases in the atmosphere results in an accompanying increase of global atmospheric temperature. Reduction of the pH of the upper ocean level is another result of accumulation of CO_2 in the atmosphere.

Large-scale storage of CO_2 in geologic formations will contribute to meet the challenge of stabilizing the concentration of CO_2 in the atmosphere. Oil, gas and condensate reservoirs are relevant locations to consider for CO_2 storage because their proven geologic seal that trapped the buoyant hydrocarbon over a geological timescale and because of the already acquired geologic description. A pre-requisite is that the geologic seal has not been damaged during the production and that the abandoned wells do not leak CO_2 to the surface[2].

In lack of petroleum reservoir for CO_2 storage purpose, deep saline formations are possible alternatives. They are more common worldwide and thus constitute a larger potential storage volume. The disadvantage is that they usually are much less characterized than petroleum reservoirs. Especially, there is normally no proven seal before injection starts.

Characterization of the aquifer is an important part of the total evaluation of the aquifer as a reliable long-term CO_2 deposit site. Detection and proper description in the simulation model of potential vertical flow barriers, topography of cap rock, faults, and other potential pathways for flow that will dominate the storage capacity and reliability of the aquifer must be considered carefully.

This paper is about storage mechanisms of CO_2 in deep saline aquifers. Gravity segregation of CO_2 towards the top of the aquifer will dominate the flow caused by the density difference between injected CO_2 and brine unless flow barriers in the aquifer restrict the vertical segregation. Large volume aquifers with reasonable permeability (to allow good injectivity), high thickness, and good communication over long distances will be the most attractive. In this setting large volumes of CO_2 can be injected without a risk of significant rise of the aquifer pressure.

The injected CO_2 will on a 1000 years time-scale diffuse into the underlying aquifer column. The resulting brine/CO_2 mixture is slightly denser than the virgin brine. This density difference will cause instability and induce convective currents in the aquifer enhancing the dissolution rate of CO_2 into the aqueous phase. The CO_2-saturated brine segregates downwards the aquifer and mixes with fresh brine. Provided a good vertical communication in the aquifer, the CO_2 will eventually dissolve in the aqueous phase and the dissolution is mainly controlled by the induced convective currents[3].

Linear stability analysis has been used to estimate the time required for this instability to occur in anisotropic permeability distribution[4]. In most cases of practical interest, the longest timescale required for complete dissolution of the injected CO_2 could be thousands of years, depending crucially on the vertical permeability of the aquifer.

Multivariable analysis has been used to study the effect of various aquifer parameters including impact of horizontal and vertical permeability, on permanent sequestration of CO_2 in conceptual aquifer model reservoir simulation[5]. The study concluded that trapping of CO_2 as a gas-water relative permeability hysteresis can impact significantly and that dissolution has a significant effect on the long-term fate of injected CO_2. The study also concluded that permeability is the primary variable affecting migration of an injected CO_2 plume and pressure buildup in the aquifer.

The Sleipner project in Norway has demonstrated the feasibility of large-scale CO_2 injection into the Utsira saline aquifer. A time-lapse 3D seismic surveying program for monitoring the CO_2 storage in the aquifer has accompanied the injection. The seismic surveying showed that the injected CO_2 flowed horizontally beneath thin shales present in the aquifer and migrating upwards through breaks in the shales towards the cap rock of the formation[6].

In this paper we will first present the different mechanisms for storing CO_2 in aquifers. Then we will give a short introduction to hysteresis in gas-water systems. Thereafter the simulation model will be presented before we present the main results. Finally we conclude upon the main findings in this study.

Mechanisms for storing CO_2 in saline formations

The following mechanisms for sequestering CO_2 in saline aquifers have been described in the literature:

CO_2 solubility in formation water. A portion of the injected CO_2 will dissolve in the formation water in the aquifer and the dissolution of CO_2 per unit volume of water is a function of pressure, temperature and salinity of the aqueous phase. The aqueous phase will contain the dissolved CO_2 regardless of being stationary or segregated/transported to another location as long as the physical conditions are un-disturbed. CO_2-saturated formation water is denser than water not containing CO_2. The difference in density of CO_2-saturated aquifer water and virgin formation water triggers convection currents in the aquifer beneath the CO_2 plume.

The dissolution of CO_2 in formation water occurs through mass transfer from CO_2 phase to aqueous phase whenever the phases are in contact. The access CO_2 phase and the aqueous phases are thereby assumed to be in thermodynamic equilibrium in the model. The amount of CO_2 dissolved in the aqueous phase as a function of the prevailing pressure, temperature and salinity in the aquifer, can be explicitly set in the simulation model by use of a realistic fluid property description based on laboratory pVT data of CO_2/brine mixtures of a wide range of proportions at various pressure and temperature conditions. This includes density and viscosity of both CO_2 and aqueous phases at pressure and temperature of relevance.

In compositional reservoir simulators the solubility of CO_2 in the aqueous phase as a function of pressure, temperature and salinity is calculated by EOS models.

Mobile CO_2 phase. Another portion of the injected CO_2 into an aquifer will be sequestered as a mobile phase of CO_2 free to move laterally or migrate (buoyant) vertically towards the cap rock of the aquifer. The cap rock constitutes a no-flow boundary or barrier like a gas trap. The phase properties of the sequestered CO_2 depend upon the prevailing pressure and temperature of the storage location of the aquifer. The critical point of CO_2 is at a temperature of 31.04°C and a pressure of 73.82 bar. At higher temperatures and/or pressures, CO_2 will exist as a supercritical fluid. At lower (subcritical) temperatures and/or pressures, CO_2 can exist in two different phase states, a liquid and a gaseous state, as well as in two-phase mixtures of these states[7].

Residual CO_2 saturation as hysteresis in gas-water saturation history. Sequestration of supercritical CO_2 as residual gas saturation in the aquifer occurs when formation water encroaches or invades the CO_2 plume. Then some of the CO_2 supercritical phase will be trapped in the pore space and a hysteresis behavior in the gas-water saturation history is experienced[8,9,10].

Mineral dissolution and carbonation. Carbonic acid is formed when CO_2 dissolves into the aquifer water. The carbonic acid reacts with various minerals in the rock matrix and dissolves reacted minerals. The dissolution products are susceptible to precipitate as stable carbonates and thereby permanently sequester a part of the injected CO_2 in the aquifer. In fact this type of CO_2 sequestration is desirable because precipitated carbonates is stagnant in the rock and could not leak into the atmosphere[11,12].

Theory of hysteresis in gas saturation history

Gas-water relative permeability hysteresis model.

Hysteresis behavior of multi-phase flow in porous media, and thereby in relative permeability and capillary pressure, originates from the difference between the advancing and receding contact angle to the present fluids against the solid surface, and from the variation of pore throat to pore body ratio and the pore size distribution. The surface of the pore walls contains different minerals with different wetting characteristics towards the present fluids in the pore structure.

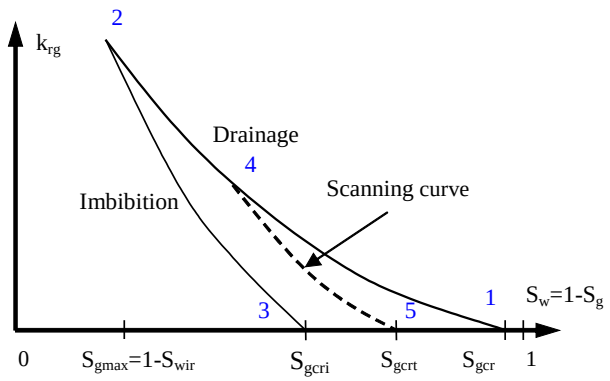

Figure 1: Relative permeability hysteresis in the non-wetting phase (after Eclipse technical manual 2003[13]).

Hysteresis in the residual gas saturation of the non-wetting phase (CO_2 supercritical gas) and hysteresis in the curve shape between drainage and imbibition relative permeability curves and capillary pressure curves are the two kinds of hysteresis effects of interest when formation water without CO_2 in solution encroaches or invades the CO_2 plume. Hysteresis in CO_2 storage in aquifers due to post-injection fluid segregation is in this study limited to hysteresis in the non-wetting phase between primary drainage and imbibition relative permeability curves as illustrated in Figure 1.

Residual saturation of the trapped CO_2 supercritical gas (non-wetting phase) is best calculated by Lands model[14]. If a reversal of the direction along the drainage relative permeability occurs during primary drainage, the residual CO_2 supercritical gas saturation is calculated from the maximum historical saturation.

An accepted pair of drainage and imbibition relative permeability curves of a non-wetting phase (gas phase) is shown in Figure 1. Gas phase is defined as the non-wetting phase; water is the wetting phase in the figure. The drainage curve represents the primary drainage relative permeability curve with gas saturation increasing from point 1 to 2, and the curve 2 to 3 represents the primary imbibition relative permeability curve. The critical saturation of the imbibition curve (S_{gcri}) is greater than that of the drainage curve (S_{gcrd}). The two curves must meet at the maximum wetting phase saturation value (S_{gmax}).

If the primary drainage process is reversed at an intermediate point 4 (S_{ghy}) by an imbibition process, a scanning curve between point 4 and 5 in the diagram is the result. The critical saturation remaining at point 5 is the trapped critical gas saturation (S_{gcrt}), which is a function of the maximum gas phase saturation reached in the run (S_{ghy})[15].

Scanning curves, k_r, p_c. Here the main formulas are presented, for more details see[13]

Relative permeability. For the non-wetting phase (CO_2) the scanning curves are calculated using Killough's method

$$k_{rg}\left(S_g\right) = \frac{k_{rg}^{imb}\left(S_{g,norm}\right)k_{rg}^{drain}\left(S_{g,hy}\right)}{k_{rg}^{drain}\left(S_{g,\max}\right)} \tag{1.1}$$

where

$$S_{g,norm} = S_{gcri} + \frac{\left(S_g - S_{gcrt}\right)\left(S_{g,\max} - S_{gcri}\right)}{S_{g,hy} - S_{gcrt}} \tag{1.2}$$

For the wetting phase (brine) no hysteresis is applied.

Capillary pressure. The scanning curves for water-gas capillary pressure are calculated from

$$p_c = p_c^{drain} + F\left(p_c^{imb} - p_c^{drain}\right) \tag{1.3}$$

where

$$F = \frac{\dfrac{1}{S_w - S_{w,hy} + E} - \dfrac{1}{E}}{\dfrac{1}{S_{w,\max} - S_{w,hy} + E} - \dfrac{1}{E}} \tag{1.4}$$

Here E is a curvature parameter, typically of order 0.1.

Simulation model

A flexible reservoir simulation model for studying CO_2 injection in a saline aquifer was constructed using a black-oil reservoir simulator. Here the oil is given water properties while CO_2 is the gas phase. The amount of CO_2 dissolved in the aqueous phase as a function of the prevailing pressure, temperature and salinity of aqueous phase in the aquifer, can be explicitly set by use of a realistic fluid property description based on laboratory pVT data of CO_2/brine mixtures of a wide range of proportions at various pressure and temperature conditions. This includes density and viscosity of both CO_2 and aqueous phases at pressure and temperature of relevance. Reservoir simulations are performed to determine the aquifer response to CO_2 injection and to study the long-term fate of the sequestered CO_2 except for mineral dissolution and carbonation.

Effective pressure. The simulator used has no simple options for including thermal gradients. To account for the temperature variation with depth a trick is therefore used by introducing an *effective, temperature adjusted pressure*. Normally both temperature and pressure increases with depth. E.g. since increased temperature reduces the viscosity while increased pressure increases it the result turns out to be a very small variation in CO_2 viscosity by the effective pressure in the reservoir where typically p=80-100 bar and T=29-36°C. In the simulations we have used

$$\begin{aligned} \mu_{CO_2}\left(p_{eff}\right) &= 0.0548 \text{ cP} \\ \mu_{\text{brine}}\left(p_{eff}\right) &= 1.2742 - 0.0052\,p_{eff} \text{ cP} \end{aligned} \tag{1.5}$$

where p_{eff} is in bar. The dependence of μ_{brine} on R_S is neglected. Reservoir density for CO_2 and brine as function of effective pressure are shown in Figure 2 and Figure 3. Note that the brine density *increases* when CO_2 dissolves.

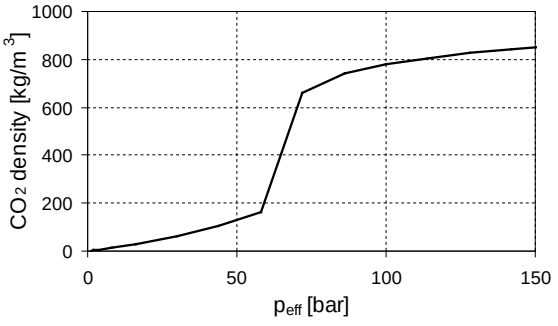

Figure 2: CO_2 density ρ_g as function of effective pressure.

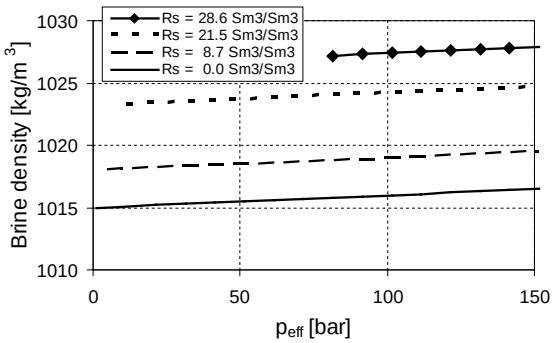

Figure 3: Brine density ρ_w for brine with dissolved CO_2 as function of effective pressure.

Boundary conditions. To mimic an infinite reservoir horizontally the pore-volume of the cells around the boundary are multiplied by a large factor (10^4).

Saturation functions. The relative permeability curves are of Corey type with exponents determined from laboratory measurements

$$k_{rw} = \left(S_w^*\right)^{\varepsilon}, \quad S_w^* = \frac{S_w - S_{wir}}{1 - S_{wir}} \tag{1.6}$$

$$k_{rg} = \left(1 - \tilde{S}_w\right)^2 \left(1 - \tilde{S}_w^{\gamma}\right), \quad \tilde{S}_w = \frac{S_w - S_{wir}}{1 - S_{wir} - S_{gr}} \tag{1.7}$$

where $S_{gr} = S_{gcrd}$ or $S_{gr} = S_{gcri}$ for drainage and imbibition respectively. Exponent values used are $\varepsilon = 4$ and $\gamma = 0.5$. Typical relative permeability curves are shown in Figure 4. For the drainage capillary pressure a van Genuchten model[16] is used

$$P_c = P_0 \left(\hat{S}_w^{-1/\lambda} - 1\right)^{1-\lambda}, \quad \hat{S}_w = \frac{S_w - S_{\ell r}}{1 - S_{\ell r}} \tag{1.8}$$

with parameters $\lambda = 0.7$ and $S_{\ell r} = S_{wir}$. For the imbibition curve a straight line tangential to the drainage curve going trough S_{gcri} and zero for higher water saturations was used, see Figure 5. The imbibition curve had to be zero above S_{gcri} to get the same trapped gas saturation for scanning curves calculated from relative permeability curves and from capillary pressure curves in ECLIPSE. However, this gives somewhat unphysical capillary pressure curves. Fortunately the effect of capillary pressure is small on reservoir scale simulation and the main properties should be captured even if the details are not strictly correct.

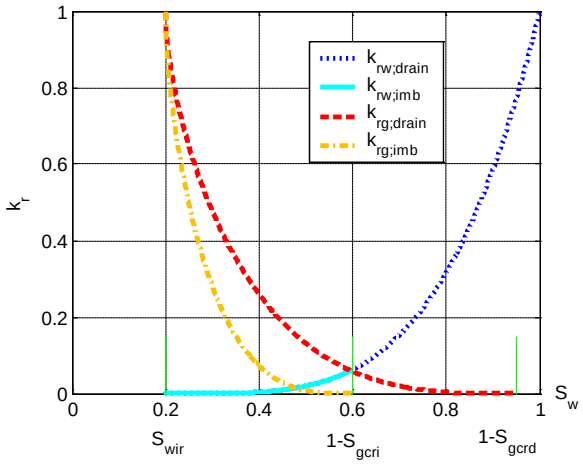

Figure 4: Typical relative permeability curves for drainage and imbibition.

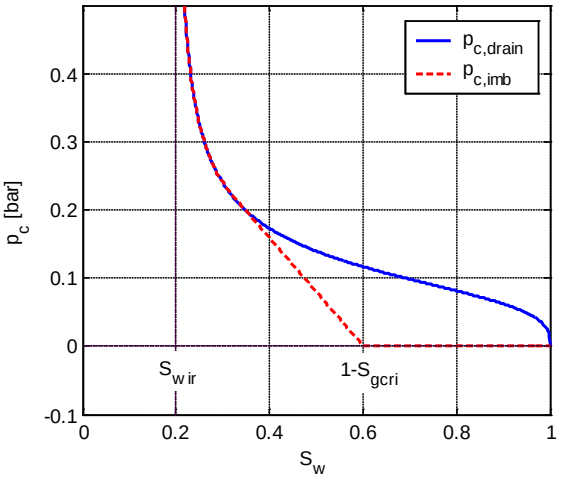

Figure 5: Typical capillary pressure for drainage and imbibition.

Trapped gas. The trapped (or residual) gas saturation is calculated using a modified version of Land's[14] and Killough's[15] method to allow nonzero S_{gcrd} as in[13]

$$S_{gcrt}\left(\vec{r},t\right) = \min\left(S_{ghy}, S_{gcrd}\right) + \max\left(0, \frac{S_{ghy} - S_{gcrd}}{A + C\left(S_{ghy} - S_{gcrd}\right)}\right) \tag{1.9}$$

where the functions min() and max() are introduced to get correct results for $S_{ghy} < S_{gcrd}$ where

$$S_{ghy} = S_{ghy}\left(\vec{r},t\right) = \max_{\tau<t} S_g\left(\vec{r},\tau\right) \tag{1.10}$$

is the highest saturation reached so far. In addition

$$A = 1 + a\left(S_{g\max} - S_{ghy}\right)$$
$$C = \frac{1}{S_{gcri} - S_{gcrd}} - \frac{1}{S_{g\max} - S_{gcrd}} \tag{1.11}$$

Here a parameter a is introduced to improve convergence, the default value is $a = 0.1$.

Since CO_2 is allowed to dissolve in water also trapped gas will dissolve in non-saturated water flowing past. As a first approximation it is assumed that trapped gas dissolves equally fast as free gas, thus

$$S_{gr}(\vec{r},t) \rightarrow S_{gr}(\vec{r},t)\xi(t) \qquad (1.12)$$

where

$$\xi(t) = \frac{V_{CO_2}^{gas}(t)}{V_{CO_2}^{gas}(t) + V_{CO_2}^{liq}(t)} \qquad (1.13)$$

A more correct method should probably have a somewhat lower dissolution rate for the trapped gas compared to the free gas.

Results and discussion

The most important simulation model parameters are summarized in Table 1.

Table 1: Simulation model parameters

Quantity	Values
Grid	20 × 20 × 20
Grid block size	300 m × 300 m × 10 m
Model size	6000 m × 6000 m × 200 m
Top of reservoir	-800 m
Porosity	25%
Permeability	k_h = 20 -2000 mD k_v = 0.2 -2000 mD
Temperature	$T_{top} \approx 29°C$, $T_{bottom} \approx 36°C$
Pressure	$p_{top} \approx 80$ bar, $p_{bottom} \approx 100$ bar
Salinity	3.0 wt.-%
Density (std. cond.)	ρ_w = 1019 kg/Sm^3 ρ_g = 1.866 kg/Sm^3
Viscosity (p=80 bar)	μ_w = 0.85 cP μ_g = 0.0548 cP
Solubility ($R_{s,max}$)	28.56 Sm^3/Sm^3
Gas formation volume factor (p=80 bar)	B_g = 0.0026 Rm^3/Sm^3
Injection rate	1.4·10^6 Sm^3/day (~10^6 tons/year)
Injection period	25 years

It is evident that many of the reservoir parameters may have an influence on how the CO_2 is distributed in the reservoir. We have focused on the following:

Grid block size. It is important to test if the results are sensitive to the resolution of the (artificial) numerical grid. The effect of doubling the number of grid blocks in each direction from 20 to 40 and reducing the size correspondingly to keep the reservoir size constant was small. All important physics thus seems to be modeled sufficiently precise with our rather coarse grid.

Effect of capillary pressure. A typical example of the effect of varying the capillary pressure scaling factor p_0 as given in Eq. (1.3) is shown in Figure 5. The effect appears to be rather small. This is as expected since capillary effects are most important at smaller scales. In the following results for different capillary pressures will be used without any special justification.

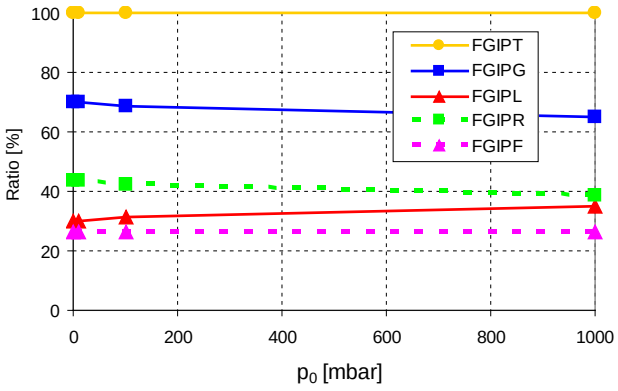

Figure 6: Effect of p_c scaling p_0 on CO_2 distribution after 1000 years for K_h=200 mD, K_v/K_h = 0.01, S_{wir}=20%, S_{grd}=5%, S_{gri}=25% (The lines are guides for the eye; simulations are performed for the points only).

Effect of critical gas saturation S_{gcrd}. Even in a model without hysteresis gas may become trapped. This is achieved by setting the critical gas saturation $S_{gcrd} = S_{gcri} > 0$. In Figure 7 a typical result is shown. As expected the amount of trapped gas increases with the critical gas saturation. Another possibility is to fix e.g. S_{gcri} = 25% and study the effect of variations in S_{gcrd}. An example is shown in Figure 8. Also here the amount of trapped gas increases with S_{gcrd}, but the effect is much smaller.

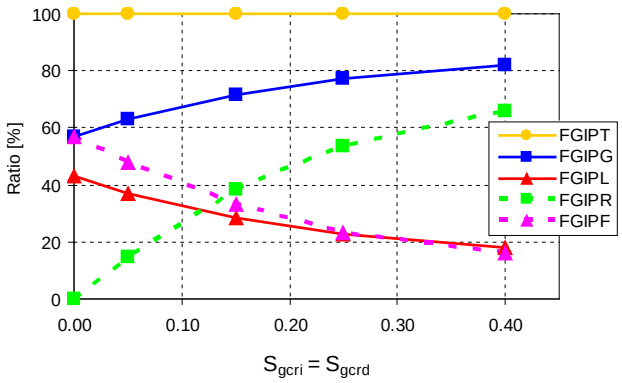

Figure 7: Effect of S_{gcri}=S_{gcrd} on CO_2 distribution after 1000 years for K_h=200 mD, K_v/K_h = 0.01, S_{wir}=20%, p_0=0 mbar.

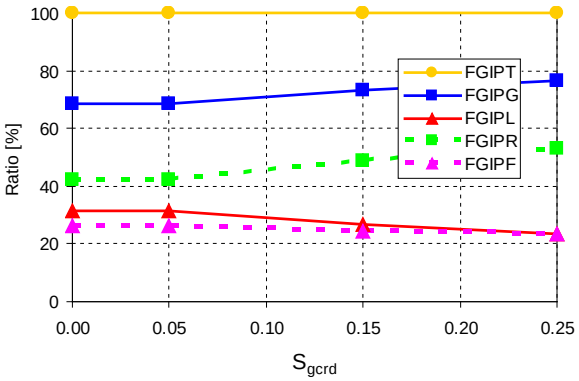

Figure 8: Effect of S_{gcrd} on CO_2 distribution after 1000 years for K_h=200 mD, K_v/K_h = 0.01, S_{wir}=20%, S_{gri}=25%, p_0=100 mbar.

Effect of S_{gcri}. To study the effect of the maximum residual gas saturation during imbibition S_{gcri} the critical gas saturation S_{gcrd} was fixed to e.g. 5%. Results for different reservoir parameters are shown in Figure 9, Figure 10, and Figure 11. It is evident that the amount of trapped gas is very dependent on S_{gcri}.

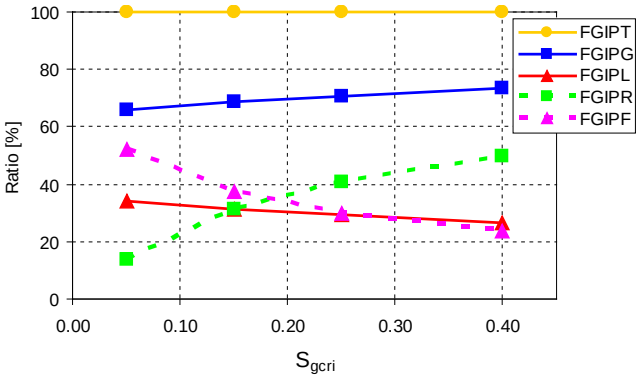

Figure 9: Effect of S_{gcri} on CO_2 distribution after 1000 years for K_h=200 mD, K_v/K_h = 0.001, S_{wir}=20%, S_{grd}=5%, p_0=100 mbar.

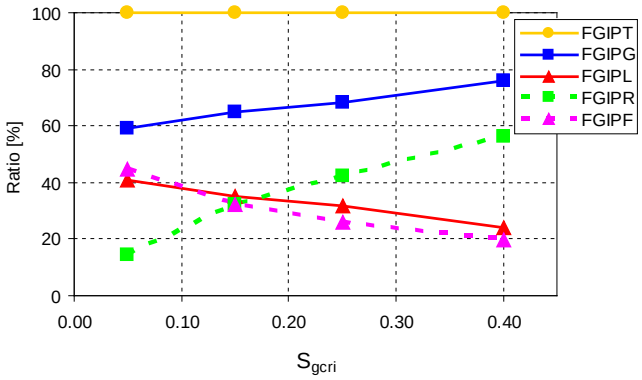

Figure 10: Effect of S_{gcri} on CO_2 distribution after 1000 years for K_h=200 mD, K_v/K_h = 0.01, S_{wir}=20%, S_{grd}=5%, p_0=100 mbar.

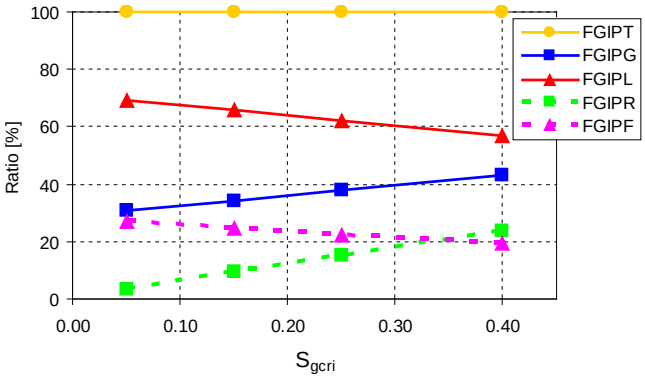

Figure 11: Effect of S_{gcri} on CO_2 distribution after 1000 years for K_h=2000 mD, K_v/K_h = 0.1, S_{wir}=20%, S_{grd}=5%, p_0=100 mbar.

Effect of irreducible water saturation S_{wir}. Since CO_2 may dissolve in water an increase in S_{wir} may have an effect in addition to an effective reduction in pore-volume. A typical result is shown in Figure 12. It may be concluded that the effect of S_{wir} is small.

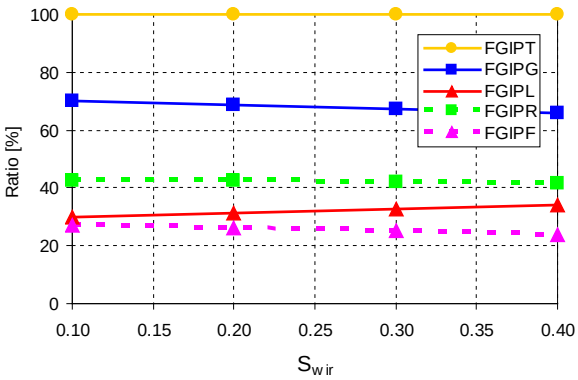

Figure 12: Effect of S_{wir} on CO_2 distribution after 1000 years for K_h=200 mD, K_v/K_h = 0.01, S_{grd}=5%, S_{gri}=25%, p_0=100 mbar.

Effect of horizontal permeability k_h. In Figure 13 the effect of varying the horizontal permeability from 20 mD to 2000 mD for a constant ratio k_v/k_h is shown. It appears that most gas is trapped for intermediate permeability values, but the overall variations are relative small.

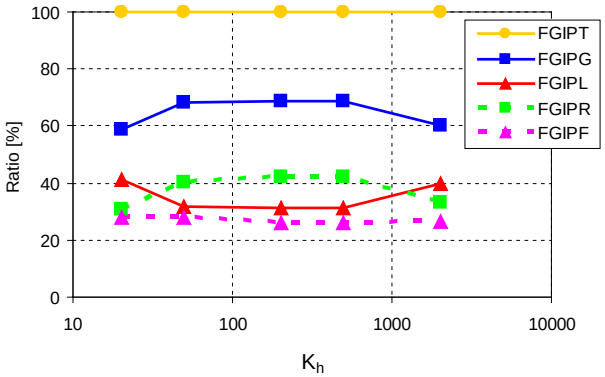

Figure 13: Effect of K_h on CO_2 distribution after 1000 years for K_v/K_h = 0.01, S_{grd}=5%, S_{gri}=25%, p_0=100 mbar.

Effect of permeability ratio k_v/k_h. In Figure 14 and Figure 15 the effects of variations in k_v/k_h are shown for k_h = 200 mD and 2000 mD respectively. It is evident that the amount of trapped gas decreases when k_v/k_h increases. In Figure 16 the time development for the models Figure 14 is shown. The difference is clearly related to the vertical migration as illustrated in Figure 17 to Figure 20. In these figures the CO_2 distribution is shown after 1000 years. The dissolved gas is related to gas saturations by using

$$S_{g,diss} = B_g \frac{1-S_g}{B_w} R_S \qquad (1.14)$$

For higher vertical permeability the amount of trapped gas decreases much faster with time. This is due to more effective mixing of brine and CO_2 resulting in more CO_2 being dissolved. This is particularly evident in Figure 20 where the lower display clearly shows convective patterns start developing. As mentioned earlier convection may strongly enhance dissolution and in fact be the most important mechanism for dissolution.

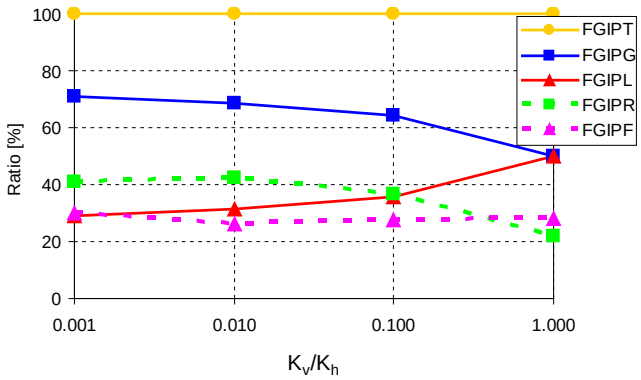

Figure 14: Effect of K_v/K_h on CO_2 distribution after 1000 years for K_h = 200 mD, S_{grd}=5%, S_{gri}=25%, p_0=100 mbar.

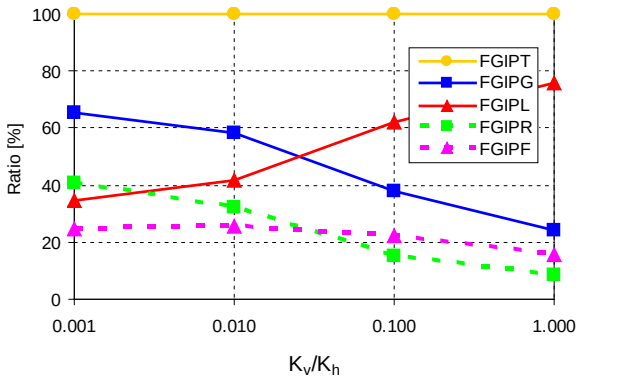

Figure 15: Effect of K_v/K_h on CO_2 distribution after 1000 years for K_h = 2000 mD, S_{grd}=5%, S_{gri}=25%, p_0=10 mbar.

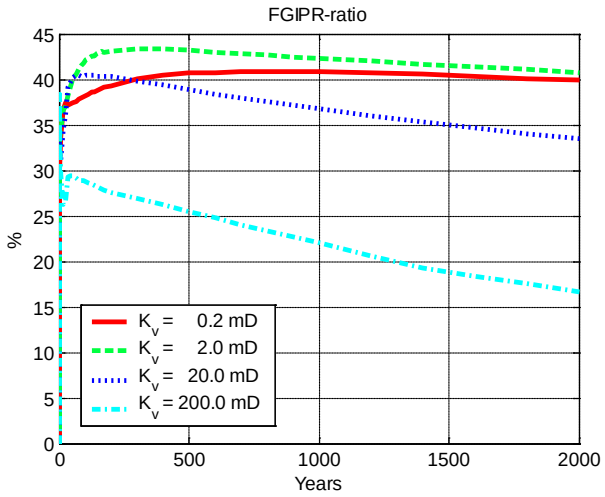

Figure 16: Effect of K_v/K_h on time development of trapped gas. Here K_h = 200 mD, S_{grd}=5%, S_{gri}=25%, p_0=100 mbar.

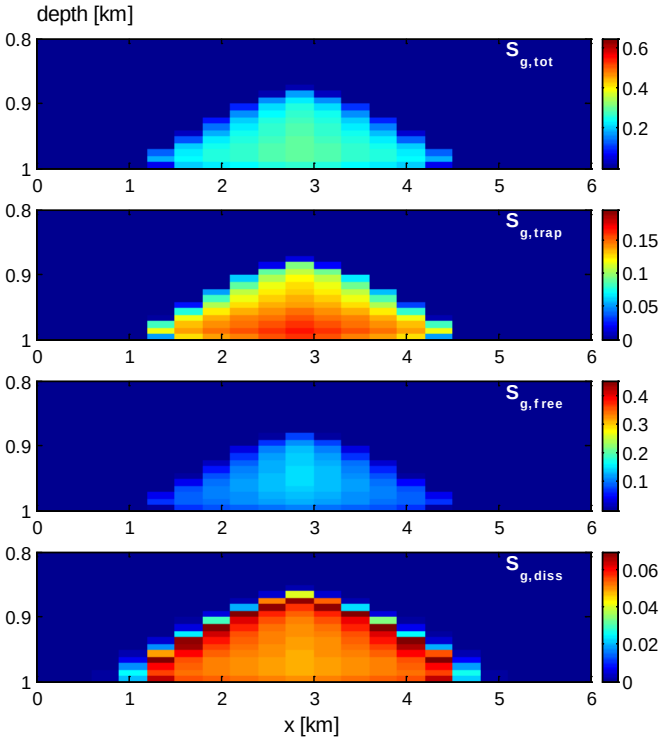

Figure 17: Cross-section of CO_2 plume after 1000 years for K_h = 200 mD, K_v/K_h=0.001, S_{wir}=20%, S_{grd}=5%, S_{gri}=25%, p_0=100 mbar. From top to bottom: S_g, $S_{g,trapped}$, $S_{g,free}$, and $S_{g,diss}$. Note that different color scale is used.

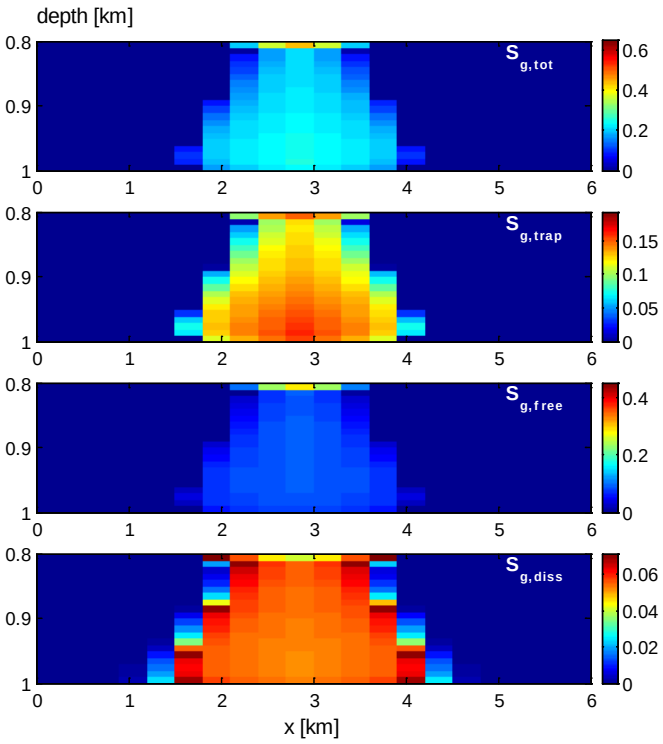

Figure 18: Cross-section of CO_2 plume after 1000 years for K_h = 200 mD, K_v/K_h=0.01, S_{wir}=20%, S_{grd}=5%, S_{gri}=25%, p_0=100 mbar. From top to bottom: S_g, $S_{g,trapped}$, $S_{g,free}$, and $S_{g,diss}$. Note that different color scale is used.

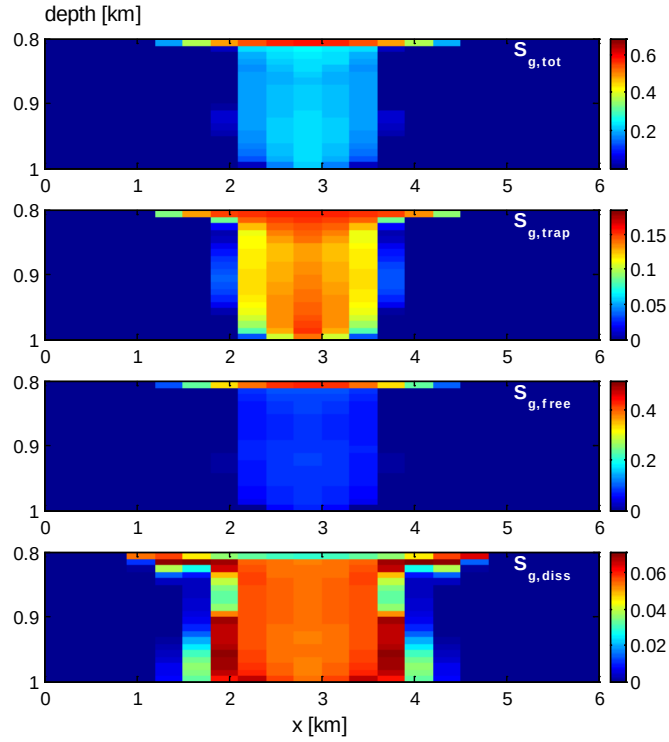

Figure 19: Cross-section of CO_2 plume after 1000 years for K_h = 200 mD, K_v/K_h=0.1, S_{wir}=20%, S_{grd}=5%, S_{gri}=25%, p_0=100 mbar. From top to bottom: S_g, $S_{g,trapped}$, $S_{g,free}$, and $S_{g,diss}$. Note that different color scale is used.

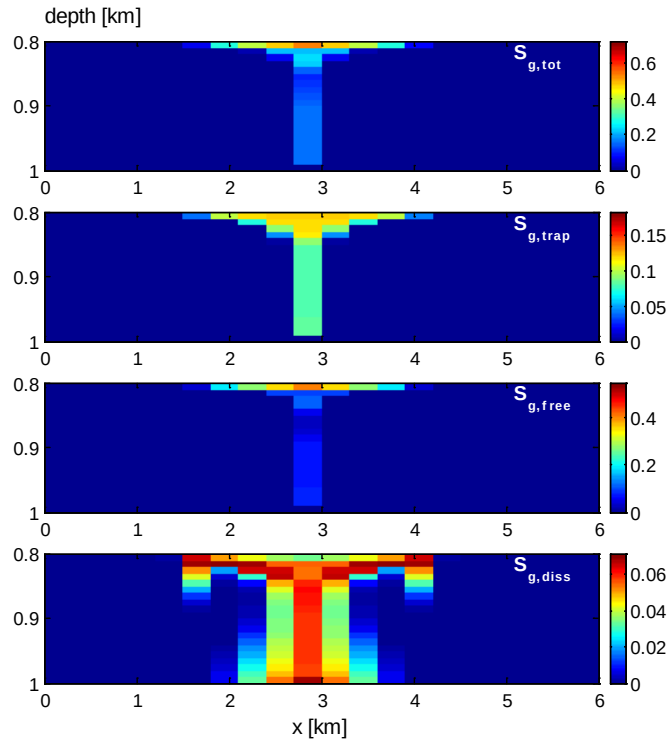

Figure 20: Cross-section of CO_2 plume after 1000 years for K_h = 200 mD, K_v/K_h=1.0, S_{wir}=20%, S_{grd}=5%, S_{gri}=25%, p_0=100 mbar. From top to bottom: S_g, $S_{g,trapped}$, $S_{g,free}$, and $S_{g,diss}$. Note that different color scale is used.

Conclusions

The following conclusions are drawn from the study.

1. A black-oil reservoir simulator with an explicit setting of pVT data of CO_2/brine mixtures and a proper setting of the process dependant dynamic reservoir parameters in a flexible reservoir simulation model is a fast and proper tool to study the aquifer response to CO_2 injection and the long-term fate of the sequestered CO_2.

2. The dissolution of CO_2 in aquifer water is the dominant mechanism of CO_2 storage in deep saline aquifers provided that the vertical communication in the aquifer allows for convective mixing of the CO_2 plume into the brine phase.

3. It is evident that the amount of trapped CO_2 gas due to the effect of gas-water capillary pressure and relative permeability hysteresis decreases when k_v/k_h increases. The percentage of trapped gas is reduced to less than 30 % at a k_v/k_h ratio of 0.1.

4. The effect of the horizontal permeability on the amount of trapped CO_2 needs further investigations. Our simulations indicate a maximum for intermediate values of k_h.

Acknowledgments

The authors gratefully acknowledge the support from the CO_2 Capture Project, CCP Phase 2 Joint Industry Project. BP Norge AS is the JIP Sub-operator for the current contract.

Nomenclature

k_{rw}	=	*relative permeability for water*
k_{rg}	=	*relative permeability for CO_2 (gas)*
μ_g	=	*CO_2 (gas) viscosity*
μ_w	=	*Water (brine) viscosity*
S_{wir}	=	*irreducible water saturation*
S_{gcrd}	=	*critical gas saturation under drainage*
S_{gcri}	=	*critical gas saturation under imbibition*
S_{gmax}	=	*maximum gas saturation (=1-S_{wr})*
S_{ghy}	=	*maximum gas saturation obtained so far*
S_{gcrt}	=	*residual/trapped gas saturation*
ε, γ	=	*Corey parameters*
p_c	=	*Capillary pressure*
p_0	=	*p_c scaling (related to entry pressure)*
λ	=	*Van Genuchten p_c parameter*
a,A,C	=	*Killough parameters*
k_h	=	*Horizontal permeability*
k_v	=	*Vertical permeability*
FGIPT	=	*Field Gas In Place Total (=FGIPG+FGIPL)*
FGIPG	=	*Field Gas In Place Gas (=FGIPR+FGIPF)*
FGIPR	=	*Field Gas In Place Residual*
FGIPF	=	*Field Gas In Place Free*
FGIPL	=	*Field Gas In Place Liquid*

SI Metric Conversion Factors

mD = $9.869 \cdot 10^{-16}$ m^2
bar = 10^5 Pa
cP = 10^{-3} Pa·s

References

1. Houghton, J.T. (ed): *Climate Change 2001: The Scientific Basis; Contribution of Working Group I to the Third Assessment Report of the Intergovernmental Panel on Climate Change*, Cambridge U. Press, New York City.
2. Orr, F.M.: "Storage of Carbon Dioxide in Geologic Formations," paper SPE 88842, Distinguished Author Series, JPT (September 2004) 90-97.
3. Lindeberg, E. and Bergmo, P.: "The Long-Term Fate of CO_2 Injected into an Aquifer," in Greenhouse Gas Control Technologies, Vol 1, J. Gale and Y. Kaya (Eds.) Elsevier Science Ltd. (2003) 489-494.
4. Ennis-King, J. and Paterson, L.: "Role of Convective Mixing in the Long-Term Storage of Carbon Dioxide in Deep Saline Formations," SPE 84344, the SPE Annual Technical Conference and Exhibition, Denver, Colorado, 5-8 October 2003.
5. Flett, M., Gurton, R. and Taggart, I.: " The Function of Gas-Water Relative Permeability Hysteresis in the Sequestration of Carbon Dioxide in Saline Formations," paper SPE 88485, the SPE Asia Pacific Oil and Gas Conference and Exhibition, Perth, Australia, 18-20 October 2004.
6. Torp, T.A. and Gale, J.: "Demonstrating Storage of CO_2 in Geological Reservoirs: The Sleipner and SACS Projects," in Greenhouse Gas Control Technologies, Vol 1, J. Gale and Y. Kaya (Eds.) Elsevier Science Ltd. (2003) 311-316.
7. Pruess, K.: "Numerical Simulation of CO_2 Leakage From a Geologic Disposal Reservoir, Including Transitions From Super- to Subcritical Conditions, and Boiling of Liquid CO_2," SPE 86098, SPEJ (June 2004), 237-248.
8. Hamon G., Suzanne K., Billiotte J., and Trocme V.: "Field-wide variations of trapped gas saturation in heterogeneous sandstone reservoirs", SPE 71524, (2001), 9 pp.
9. Holtz M.H., "Residual gas saturation to aquifer influx: a calculation method for 3-d computer reservoir model construction", SPE 75502, (2002), 10 pp.
10. Kumar A., Noh M., Pope G.A., Sepehrnoori K., Bryant S., and Lake L.W.: "Reservoir simulation of CO_2 storage in deep saline aquifers", SPE 89343, (2004), 10 pp.
11. Pruess, K., Xu, T., Apps, J. and Garcia, J.: "Numerical Modeling of Aquifer Disposal of CO_2," SPE 88485, SPEJ (March 2003), 49-60.
12. Nghiem, L., Shrivastava, V., Kohse, B. and Sammon, P.: "Simulation of CO_2 EOR and Sequestration Processes with a Geochemical EOS Compositional Simulator," Paper 2004-051, the Petroleum Society's 5th Canadian International Petroleum Conference, Calgary, Alberta, Canada, June 8-10, 2004.
13. Eclipse Technical Manual 2003.
14. Land C.S., "Calculation of Imbibition Relative Permeability for Two- and Three-Phase Flow from Rock Properties," SPEJ, (June 1968), 149-156, SPE 1942.
15. Killough, J.E.: "Reservoir Simulation with History-dependent Saturation Functions," Trans AIME 261, (1976), p 37-48, SPE 5106.
16. van Genuchten, M.T.: "A Closed-Form Equation for Predicting the Hydraulic Conductivity of Unsaturated Soils", Soil Sci. Soc. Am. J. (1980) **44**, 892.